phys. stat. sol. (a) **202**, No. 9, 1758–1762 (2005) / **DOI** 10.1002/pssa.200520031

Characteristics of SnO_2 fishbone-like nanostructures prepared by the thermal evaporation

Hyoun Woo Kim*, **Nam Ho Kim, Ju Hyun Myung,** and **Seung Hyun Shim**

School of Materials Science and Engineering, Inha University, Incheon 402-751, Republic of Korea

Received 8 January 2005, revised 4 March 2005, accepted 10 March 2005
Published online 9 May 2005

PACS 61.10.Nz, 68.37.Lp, 68.55.Jk, 81.05.Hd, 81.15.Ef

We have successfully grown the tin oxide (SnO_2) fishbone-like nanostructures on titanium nitride (TiN)-coated substrates by the thermal evaporation of Sn powders. X-ray diffraction indicated that the product had the phase structure of the rutile form of SnO_2. Transmission electron microscopy (TEM) revealed that the product consisted of fishbone-like structure, with branches and sub-branches attached to the main stem. High-resolution TEM and selected area diffraction pattern coincidentally indicated that both branches and sub-branches were single crystalline rutile SnO_2 structures. Room temperature photoluminescnece (PL) spectrum of the as-synthesized SnO_2 nanostructures exhibited peaks associated with the visible light emission.

1 Introduction

Tin dioxide (SnO_2) is an n-type semiconductor with a wide band gap (E_g = 3.62 eV, at 300 K) and is well known for its potential applications in gas sensors [1], dye-based solar cells [2], transparent conducting electrodes [3], and catalyst supports [4]. Because nanoscale one-dimensional (1-D) structures have attracted great deal of interest owing to their unique electronic, optical, and mechanical properties as a result of their low dimensionality and the quantum confinement effect [5, 6], various structural and morphological forms of SnO_2 1-D nanomaterials have been fabricated over the past several years, including nanowires [7–9], nanoribbons [10–13], nanorods [14–16], nanodendrites [17, 18], and nanobelts [19].

In this study, the SnO_2 fishbone-like nanostructures were prepared and characterized. Although J. Q. Hu et al. previously reported the production of a SnO_2 fishbone-like structure via the thermal evaporation of Sn powders using $Fe_3(NO_3)_3$ as the oxidizing agent at 1100 °C [20], we have employed a simple thermal evaporation of Sn powders in the presence of flowing O_2 flow at a lower temperature of 900 °C.

2 Experimental

Figure 1 shows the sketch of the apparatus used. An alumina boat with the Sn powders (purity: 99.9%) was placed into a quartz tube in a furnace. On top of the boat, a piece of the substrate was placed with the titanium nitride (TiN)-coated side facing downwards. The powder-to-TiN substrate distance was approximately 10 mm. Prior to evaporation, the tube was evacuated to 0.01 Torr using a mechanical pump. During the experiment, a constant pressure with an oxygen (O_2) flow was maintained at 1 Torr. The temperature near the substrate was approximately 900 °C and the experimental time was 2 hours.

* Corresponding author: e-mail: hwkim@inha.ac.kr, Phone: +82 32 860 7544, Fax: +82 32 862 5546

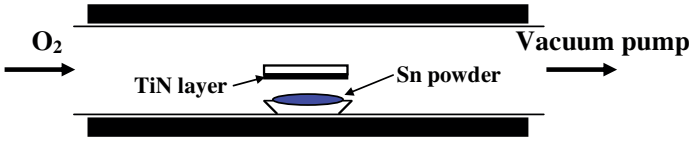

Fig. 1 (online colour at: www.pss-a.com) Schematic diagram of the apparatus used in experiment.

After evaporation, the substrate was cooled and then removed from the furnace for structural characterization.

The structural properties of the as-grown products were investigated using grazing angle X-ray diffraction (XRD: CuKα_1 radiation) (Philips X'pert MRD) with an incidence angle of 0.5° and transmission electron microscopy (TEM, Philips CM-200) with energy-dispersive X-ray spectroscopy (EDS) installed. The TEM specimens were prepared by sonicating the samples in acetone, and subsequently dropping the solution onto a holey carbon film supported on a copper grid. The photoluminescence (PL) measurement was performed at room temperature using a He–Cd laser line of 325 nm as the excitation source.

3 Results and discussion

Figure 2 shows the typical XRD pattern of the as-synthesized product. Miller indices are indicated on each diffraction peak. The reflection peaks of (110), (101), (200), (211), (220), (310), (112), (301), (202), and (321) can be readily indexed to a tetragonal rutile structure of SnO_2 with lattice constants $a = 4.734$ Å and $c = 3.185$ Å (JCPDS Card File No. 41-1445). The strong and sharp reflection peaks suggest that the as-synthesized products are well crystallized. No obvious reflection peaks from impurities, such as unreacted Sn or other tin oxides, can be detected. In our XRD measurements, the angle of the incident beam to the substrate surface was about 0.5°, and a detector rotated to scan the samples. Therefore, we surmise that the peaks are mainly from the products. The XRD analyses indicate that the well-crystallized SnO_2 products were successfully obtained through the present synthetic route.

We have examined the overall morphology of the products by TEM. As shown in Fig. 3a, the product consists of fishbone-like structures, which displays numerous characteristic branches and sub-branches attached to a single main stem. Close examination reveals that the fishbone-like structure has twofold structural symmetry, in which two rows of branches, which are opposite in direction, grow on the major stem and almost perpendicular to the major stem. These branches have almost uniform diameters along the length direction, in the range of 50–250 nm. It is noteworthy that no particles are observed at the tip ends of both branches and sub-branches. The EDS analysis indicated that the synthesized products consist of only Sn and O elements, regardless of position in the fishbone-like structure. The associated EDS

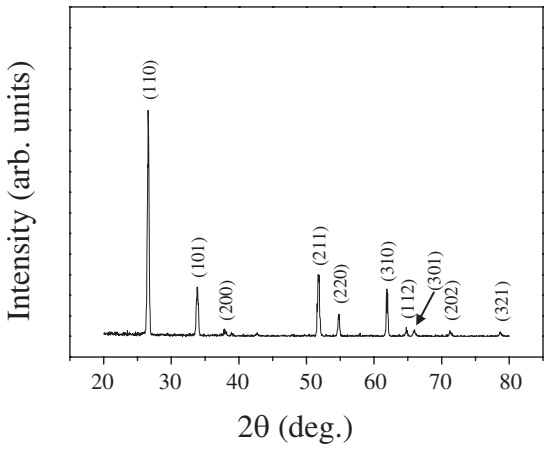

Fig. 2 XRD pattern of the products.

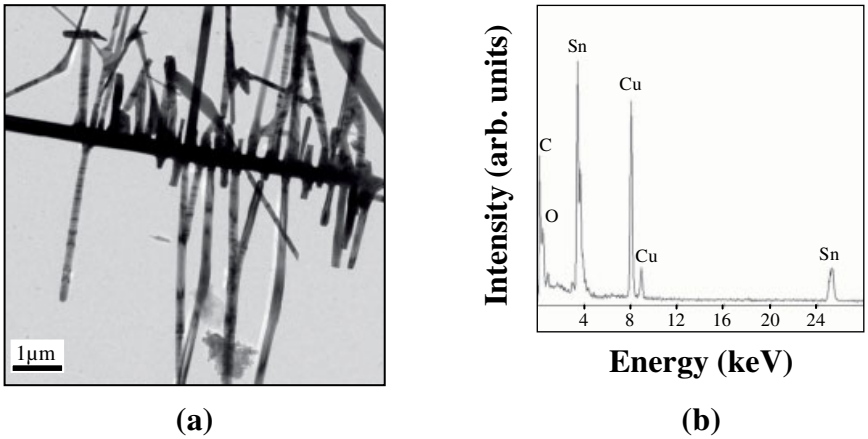

Fig. 3 (a) TEM image showing a segment of the fishbone-like nanostructure. (b) The corresponding EDS spectrum.

spectrum is shown in Fig. 3b. The C- and Cu-related signals, respectively, are due to the contamination of C while preparing TEM specimens and due to the presence of Cu grids.

Figure 4a shows a TEM image of the individual branch. The corresponding selected area electron diffraction (SAED) pattern (Fig. 4a, upper left inset) can be indexed to be $[11\bar{3}]$ zone axis of the rutile structured SnO_2 crystal. An HRTEM image taken near the edge along this branch is shown in Fig. 4b. As seen from the image, this branch is structurally uniform single crystalline. The interplanar spacing is approximately 0.34 nm, corresponding to the $(1\bar{1}0)$ plane of ruile SnO_2. The growth direction of the branch is parallel to the [301] crystalline orientation of SnO_2. The SAED pattern (shown in Fig. 5b) recorded on the entire sub-branch (shown in Fig. 5a) reveals the single-crystalline nature of the sub-branch in the fishbone-like structure. The SAED pattern can be indexed for the [001] zone axis of crystalline SnO_2. From HRTEM images (shown in Fig. 5c and 5d), we find that the stem and the sub-branch have the same crystalline orientation. Figure 5c and 5d coincidentally indicate that the interplanar spacings are about 0.47 nm, corresponding to the (010) or (100) planes of rutile SnO_2.

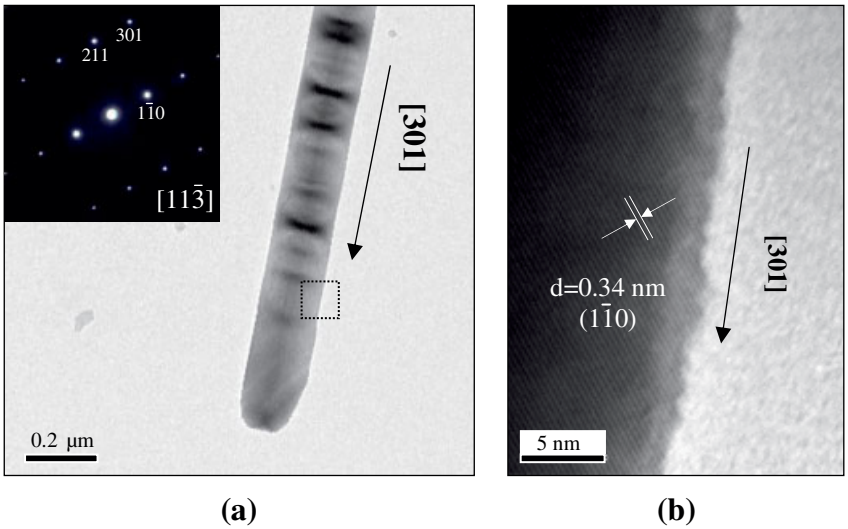

Fig. 4 (a) TEM image of a single branch (Inset: Corresponding SAED pattern recorded). (b) HRTEM image of the area marked in (a).

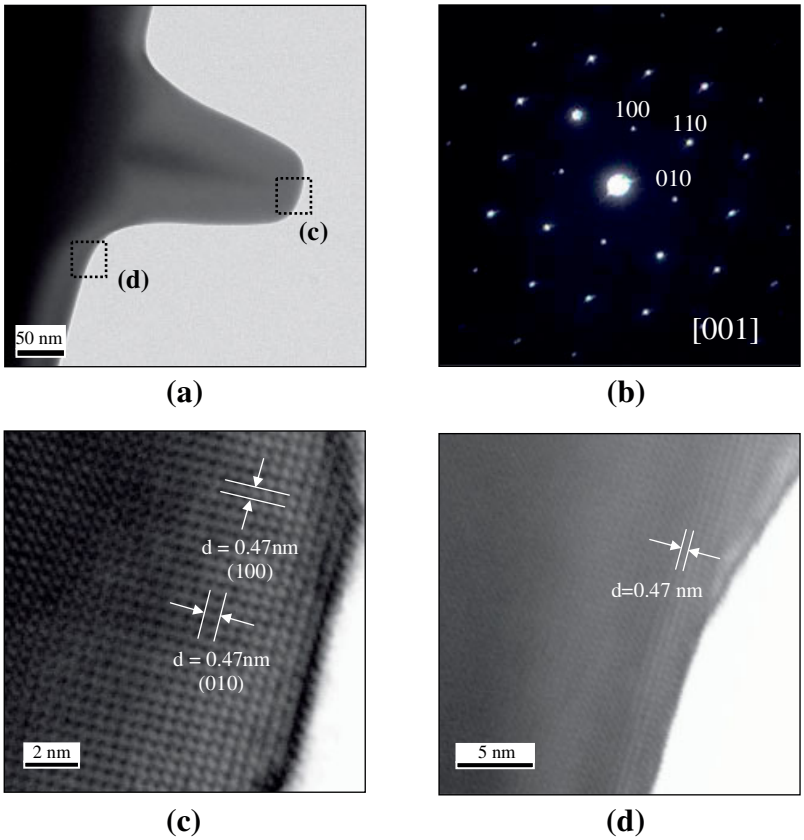

Fig. 5 (a) TEM image of a single sub-branch. (b) SAED pattern recorded on the entire sub-branch in (a). (c, d) HRTEM images recorded in different regions of the sub-branch in (a).

When the synthesis was carried out under the same conditions on conventional Si or gold (Au) substrates, no 1-D nanostructure was obtained. Therefore, the TiN layer affects the formation of the SnO_2 nanostructures in this synthesis route. Since SEM images and EDS measurements indicate that the nanostructure tips are free of metal particles, it is believed that the growth of the SnO_2 nanostructure in the present route is not dominated by a tip-growth vapor-liquid-solid mechanism. In this case, O_2 might work as both a reactant and a carrier gas. The Sn atoms from the Sn powders reacts with O_2 to form a metastable SnO, which subsequently decomposes into SnO_2 and Sn [21]. It is believed that the precipi-

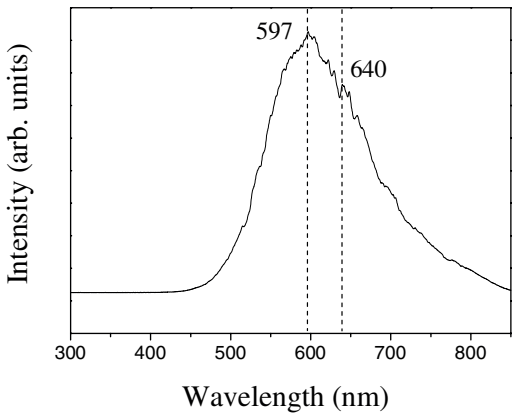

Fig. 6 Room temperature PL spectrum of the products.

tated solid SnO_2 acts as a nucleus for the SnO_2 nanostructures. Intensive investigations will be needed to reveal not only the basic reactions involved in the formation of the SnO_2 nanostructures but also the role of TiN working their formation.

Figure 6 shows a room temperature PL spectrum of the as-synthesized product. There is an apparent broad, strong emission PL band, which can be a superimposition of several peaks. The dominant emission peak is located at a wavelength of around 597 nm, corresponding to the energy of about 2.08 eV in the yellow region. It is noteworthy that there is an emission shoulder at the energy of 1.94 eV (λ = 640 nm) in the orange region. Both yellow and orange luminescence are known to be associated with defect energy levels within the band gap of SnO_2 [22–24]. Further systematic study in underway in order to reveal the mechanism of observed emissions.

4 Conclusions

We have characterized the single-crystalline SnO_2 fishbone-like nanostructures by XRD, TEM, and SAED. The product has the phase structure of the rutile form of SnO_2. The product consists of fishbone-like structure, with branches and sub-branches attached to the main stem. Both branches and sub-branches are single crystalline SnO_2 structures. The length direction of the branch is parallel to the [301] crystalline orientation of SnO_2. The PL spectrum under excitation at 325 nm shows a broad band with a prominent emission peak around 597 nm.

Acknowledgements This work was supported by grant No. R05-2004-000-10762-0 from the Basic Research Program of the Korea Science & Engineering Foundation.

References

[1] E. R. Leite, I. T. Weber, E. Longo, and J. A. Varela, Adv. Mater. **12**, 966 (2000).
[2] S. Ferrere, A. Zaban, and B. A. Gsegg, J. Phys. Chem. B **101**, 4490 (1997).
[3] Y. S. He, J. C. Campbell, R. C. Murphy, M. F. Arendt, and J. S. Swinnea, J. Mater. Res. **8**, 3131 (1993).
[4] W. Dazhi, W. Shulin, C. Jun, Z. Suyuan, and L. Fangqing, Phys. Rev. B **49**, 282 (1994).
[5] K. Himura, M. Yazawa, T. Katsuyama, K. Haraguchi, K. Ogawa, and M. Kouguchi, J. Appl. Phys. **77**, 447 (1995).
[6] J. D. Justin, K. P. Johnston, R. C. Doty, and B. A. Korgel, Science **287**, 1471 (2000).
[7] M. Zhang, G. Li, X. Zhang, S. Huang, Y. Lei, and L. Zhang, Chem. Mater. **13**, 3859 (2001).
[8] R.-Q. Zhang, Y. Lifshitz, and S.-T. Lee, Adv. Mater. **14**, 1029 (2003).
[9] A. Kolmakov, Y. Zhang, G. Cheng, and M. Moskovits, Adv. Mater. **15**, 997 (2003).
[10] Z. R. Dai, Z. W. Pan, and Z. L. Wang, Solid State Commun. **118**, 351 (2001).
[11] Z. L. Wang and Z. Pan, Adv. Mater. **14**, 1029 (2002).
[12] J. Q. Hu, X. L. Ma, N. G. Shang, Z. Y. Xie, N. B. Wong, C. S. Lee, and S. T. Lee, J. Phys. Chem. B **106**, 3823 (2002).
[13] X. S. Peng, L. D. Zhang, G. W. Meng, Y. T. Tian, Y. Lin, B. Y. Geng, and S. H. Sun, J. Appl. Phys. **93**, 1760 (2003).
[14] Y. Liu, C. Zheng, W. Wang, C. Yin, and G. Wang, Adv. Mater. **13**, 1883 (2001).
[15] C. Xu, G. Xu, Y. Liu, X. Zhao, and G. Wang, Sci. Mater. **46**, 789 (2002).
[16] D.-F. Zhang, L.-D. Sun, J.-L. Yin, and C.-H. Yan, Adv. Mater. **15**, 1022 (2003).
[17] J. K. Jian, X. L. Chen, W. J. Wang, L. Dai, and Y. P. Xu, Appl. Phys. A **76**, 291 (2003).
[18] Y.-J. Ma, F. Zhou, L. Li, and Z. Zhang, Solid State Commun. **130**, 313 (2004).
[19] S. H. Sun, G. W. Meng, Y. W. Wang, T. Gao, M. G. Zhang, Y. T. Tian, X. S. Peng, and L. D. Zhang, Appl. Phys. A **76**, 287 (2003).
[20] J. Q. Hu, Y. Bando, and D. Goldberg, Chem. Phys. Lett. **372**, 758 (2003).
[21] J. Q. Hu, X. L. Ma, N. G. Shang, Z. Y. Xie, N. B. Wong, C. S. Lee, and S. T. Lee, J. Phys. Chem. B **106**, 3823 (2002).
[22] D. Cai, Y. Su, Y. Chen, J. Jiang, Z. He, and L. Chen, Mater. Lett., in press.
[23] D. Maestre, A. Cremades, and J. Piqueras, J. Appl. Phys. **95**, 3027 (2004).
[24] S.-S. Chang and D. K. Park, Mater. Sci. Eng. B **95**, 55 (2002).